

Reaction Mechanism and Regioselectivity of the Bingel-Hirsch Addition of Dimethyl Bromomalonate to La@C_{2v}-C₈₂

Juan Pablo Martínez,^a Marc Garcia-Borràs,^a Sílvia Osuna,^a Jordi Poater,^{b,c,d} F. Matthias Bickelhaupt,^{*,b,e} Miquel Solà^{*,a}

^a Institut de Química Computacional i Catàlisi and Departament de Química, Universitat de Girona, Campus de Montilivi, 17071 Girona, Catalonia, Spain, email: Miquel.Sola@udg.edu.

^b Department of Theoretical Chemistry and Amsterdam Center for Multiscale Modeling, Vrije Universiteit Amsterdam, De Boeleaan 1083, NL-1081 HV Amsterdam, The Netherlands, email: F.M.Bickelhaupt@vu.nl.

^c Departament de Química Orgànica, Universitat de Barcelona, Martí i Franquès 1-11, 08028 Barcelona, Catalonia, Spain

^d Institució Catalana de Recerca i Estudis Avançats (ICREA), Pg. Lluís Companys, 08010 Barcelona, Catalonia, Spain

^e Radboud University Nijmegen, Institute for Molecules and Materials, Heyendaalseweg 135, 6525 AJ Nijmegen, The Netherlands.

Abstract

We have quantum chemically explored the thermodynamics and kinetics of all 65 possible mechanistic pathways of the Bingel-Hirsch addition of dimethyl bromomalonate to the endohedral metallofullerene La@C_{2v}-C₈₂ using dispersion-corrected DFT that result from the combination of 24 nonequivalent carbon atoms and 35 different bonds present in La@C_{2v}-C₈₂. Experimentally, this reaction leads to four singly-bonded derivatives and one fulleroid adduct. Out of these five products, only the singly-bonded derivative on C23 could be unambiguously identified. Our calculations show that La@C_{2v}-C₈₂ is not particularly regioselective under Bingel-Hirsch conditions. From the obtained results, however, it is possible to make a tentative assignment of the products experimentally observed. We propose that the observed fulleroid adduct results from the attack to bond **19** and that the singly-bonded derivatives correspond to the C2, C19, C21, and C23 initial attacks. However, other possibilities cannot be ruled out completely.

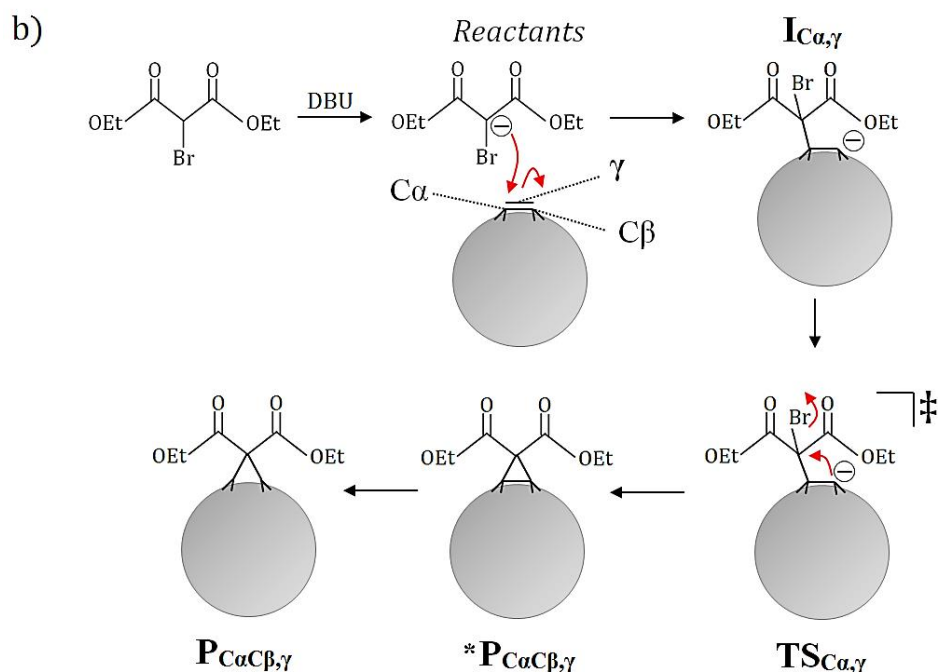
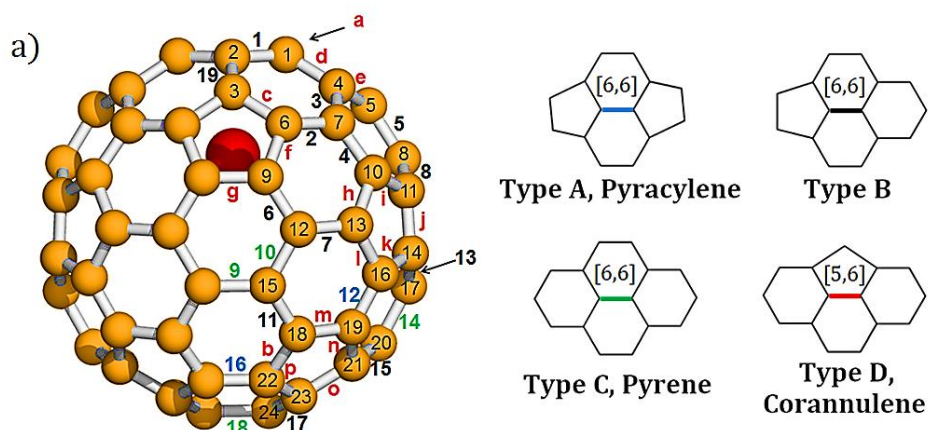
1. Introduction

The encapsulation of metallic clusters into fullerene cages led to the discovery of endohedral metallofullerenes (EMFs),^[1-7] materials with a large number of promising applications in the fields of biosciences as biocides,^[8] medical sciences as photoactive nanoparticles with uses in radiotherapy,^[9] molecular electronics as molecular switching devices,^[10] and photovoltaics as charge carriers in dye-sensitized solar cells.^[11]

Motivated by the first detection of La@C₆₀, Smalley and coworkers^[12] were able to produce macroscopic quantities of higher fullerenes with La inside the cage, including La@C₈₂. There are nine distinct isomers of C₈₂ satisfying the so-called isolated pentagon rule (IPR).^[13-15] Out of these nine cages, La as a single metal has been incarcerated into the C_{2v}-C₈₂ and C_s-C₈₂ IPR cages.^[16] None of these isomers is the most stable for empty C₈₂ fullerene. The La@C_{2v}-C₈₂ EMF, which in the case of Ce@C_{2v}-C₈₂ is approximately four times more abundant than its analogous C_s-C₈₂,^[17] has been the subject of many studies.^[18-20] For example, the first EMF functionalization was achieved for La@C_{2v}-C₈₂ through a photochemical reaction with disilirane.^[21]

Electronic and structural properties of the La@C_{2v}-C₈₂ cage have been already studied. According to the ionic model,^[22-25] charge transfer from the La atom to the fullerene cage occurs and, as a result, the formal electronic structure of La@C_{2v}-C₈₂ is described as La³⁺@C_{2v}-C₈₂³⁻, with a number of unpaired electrons located on the fullerene cage. In this regard, La@C_{2v}-C₈₂ has the capability to easily donate and, in turn, accept electrons due to its radical nature and redox properties; unlike the pristine counterpart C_{2v}-C₈₂. Consequently, the high electron affinity and low ionization potential of amphoteric species such as La@C_{2v}-C₈₂ are useful to control the chemical reactivity towards nucleophiles and electrophiles.^[26] Additionally, the permanent magnetic moment of La@C_{2v}-C₈₂ obstructs the direct application of nuclear magnetic resonance (NMR) analysis; therefore the corresponding spectrum is obtained from La@C_{2v}-C₈₂⁻ taking advantage of its uncommon stability.^[27] The ¹³C NMR spectrum of La@C_{2v}-C₈₂⁻ shows 24 different lines corresponding to 24 nonequivalent carbon atoms. In line with these results, by using synchrotron powder diffraction, the maximum entropy method (MEM)/Rietveld analysis revealed that the La atom is not localized at the center of the C₂ axis but adjacent to a six-membered ring (6-MR) of the La@C_{2v}-C₈₂ cage, the shortest La-C distance was determined to be 2.55 Å.^[28] Lastly, by taking into consideration the symmetry of La@C_{2v}-C₈₂, it is possible to differentiate 19 [6,6] and 16 [5,6] different bonds (see Scheme 1a).

Scheme 1. a) The 24 nonequivalent carbon atoms and the 35 different bonds of $\text{La}@C_{2v}\text{-C}_{82}$. For bonds, numbers denote [6,6] bonds and lower-case letters denote [5,6] bonds. Bond types are distinguished by color code (type A: blue, type B: black, type C: green, type D: red). Labels as assigned in a previous study.^[18] b) General mechanism of the nucleophilic [2+1] Bingel-Hirsch reaction in $\text{La}@C_{2v}\text{-C}_{82}$. Nomenclature used in the current work is also provided. The attack on a bond γ formed between adjacent carbon atoms C_α and C_β leads to the formation of an intermediate, either $\text{I}_{C_\alpha,\gamma}$ or $\text{I}_{C_\beta,\gamma}$; thus proceeding to the respective transition state, either $\text{TS}_{C_\alpha,\gamma}$ or $\text{TS}_{C_\beta,\gamma}$, which leads to the formation of a methanofullerene $^*\text{P}_{C_\alpha C_\beta,\gamma}$ or fulleroid $\text{P}_{C_\alpha C_\beta,\gamma}$.



$$\gamma = 1, 2, 3, \dots, 19, a, b, c, \dots, p$$

$$\alpha \text{ or } \beta = 1, 2, 3, \dots, 24$$

Chemical functionalization of EMFs^[5,6] is commonly achieved through cycloaddition reactions, being the most important: Diels-Alder,^[18,29] 1,3 dipolar (or Prato),^[30] and nucleophilic [2+1] Bingel-Hirsch (BH) additions.^[31–33] The BH addition is a cyclopropanation reaction where a fullerene and diethyl bromomalonate in the presence of a strong base such as 1,8-diazabicycloundec-7-ene (DBU) or sodium hydride react to produce a methanofullerene or a fulleroid.^[34] In the first step of the mechanism, the base abstracts the acidic proton of the malonate derivative to generate a carbanion or enolate. Then this carbanion nucleophilically attacks the fullerene, thus generating a new carbanion with charge localized at the cage. In the final step, bromide is displaced in a nucleophilic substitution S_N2 reaction causing an intramolecular three-membered ring closure. Scheme 1b illustrates the mechanism of the BH reaction in La@C_{2v}-C₈₂, in which we have introduced the nomenclature used through the whole manuscript. Accordingly, the initial attack on bond γ formed between adjacent carbon atoms C α and C β leads to the formation of a singly-bonded derivative which is labeled as the intermediate structure, either **I**_{C α , γ} or **I**_{C β , γ} , followed by the corresponding transition state structure, either **TS**_{C α , γ} or **TS**_{C β , γ} , leading to the formation of a closed-cage Bingel product methanofullerene ***P**_{C α C β , γ} or an open-cage fulleroid **P**_{C α C β , γ} . Moreover, since there are 19 [6,6] and 16 [5,6] different bonds in La@C_{2v}-C₈₂, γ can take 35 different values; on the other hand, there are 24 different values for either C α or C β because of the 24 nonequivalent carbon atoms forming the cage.

The first successful functionalization of EMFs through the BH reaction was achieved by Alford and co-workers, wherein Gd@C₆₀[C(COOC₂H₅)_n (*n* = 1-10) was the main product.^[35] The same procedure applied to ²¹²Pb@C₆₀ led to the formation of ²¹²Pb@C₆₀[C(CO₂H)₂]_x.^[36] In 2005, Echegoyen *et al.*^[37] reported the selective BH formation of Y₃N@I_h-C₈₀ and Er₃N@I_h-C₈₀ [6,6] monoadducts under mild conditions.^[38] In some cases [6,6]-products could be further converted to [5,6]-adducts by heating. The same authors also noticed that the BH reaction did not take place in Sc₃N@I_h-C₈₀ and Lu₃N@I_h-C₈₀ under the same reaction conditions.^[37] X-ray structure of Y₃N@I_h-C₈₀[C(CO₂CH₂Ph)₂] confirmed that the BH monoadduct was the result of the attack to a [6,6] bond that leads to the formation of a fulleroid structure with one of the yttrium atoms directly pointing to the attacked open bond.^[39] DFT calculations indicated that the open [6,6] adduct is more stable than the closed one and that the rotation of the metallic cluster inside the cage is partially hindered once the adduct is formed.^[39] Later, in 2010, Echegoyen and coworkers reported that Sc₃N@I_h-C₈₀ and Lu₃N@I_h-C₈₀ can undergo BH additions to yield open [6,6] adducts by changing the common BH reaction conditions. NaH was used as the base and a 4:1 mixture of *o*-DCB and N,N-dimethylformamide as the solvent.^[40] Interestingly, the BH reaction of TiSc₂N@I_h-C₈₀ afforded two unconventional singly bonded monoadducts, revealing a change

in the addition pattern and an improved reactivity of $\text{TiSc}_2\text{N}@I_h\text{-C}_{80}$ when compared to $\text{Sc}_3\text{N}@I_h\text{-C}_{80}$.^[41] A study of the BH reaction of $\text{Gd}_3\text{N}@C_{80}$, $\text{Gd}_3\text{N}@C_{84}$, and $\text{Gd}_3\text{N}@C_{88}$ performed by Echegoyen *et al.* led to the conclusion that EMFs reactivity is reduced when the size of the fullerene cage increases.^[42] BH additions to non-IPR cages have been experimentally achieved for $\text{Sc}_3\text{N}@D_3(6140)\text{-C}_{68}$,^[43] $\text{Gd}_3\text{N}@C_s(39663)\text{-C}_{82}$, and $\text{Gd}_3\text{N}@C_s(51365)\text{-C}_{84}$ EMFs.^[42,44] For the former, according to theoretical studies^[45] and experiments,^[43] the addition takes place at a [6,6] bond close to a [5,5] bond and to the Sc atom. For the other systems,^[42,44] the BH addition occurred on a [5,6] bond adjacent to the unique [5,5] bond. Unexpectedly, the addition never took place on the *a priori* more reactive [5,5] bond. This result was attributed to the larger aromaticity of the adducts of the [6,6]- and [5,6]-additions to the $\text{Sc}_3\text{N}@D_3(6140)\text{-C}_{68}$ and $\text{Gd}_3\text{N}@C_s(51365)\text{-C}_{84}$ EMFs, respectively.^[46] It is worth mentioning that theoretical studies of the reaction mechanism of BH additions to $\text{Sc}_3\text{N}@I_h\text{-C}_{80}$ and $\text{Sc}_3\text{N}@D_3(6140)\text{-C}_{68}$ ^[45] and to $\text{Y}_3\text{N}@C_s(39663)\text{-C}_{82}$ and $\text{Y}_3\text{N}@C_s(51365)\text{-C}_{84}$ ^[47] were performed by Poblet and co-workers. Their results show that the BH thermodynamic and kinetic products do not coincide, being the kinetically controlled product the one observed under experimental conditions. Very recently, some of us in collaboration with Echegoyen's group have studied experimentally and theoretically the BH to $\text{Sc}_3\text{N}@D_{5h}\text{-C}_{80}$.^[48] Our results show that the addition takes place under kinetic control in a [6,6] bond and confirm that the most stable thermodynamic and kinetic products differ.

The BH addition to $\text{La}@C_{2v}\text{-C}_{82}$ was experimentally explored by Nagase, Akasaka, and co-workers^[20,49,50] using diethyl bromomalonate as a reactant. The BH reaction was monitored by multistage high-performance liquid chromatography (HPCL), which allowed the identification of different monoadducts. They could isolate four ESR-inactive adducts, which were assigned to singly-bonded products, and one ESR-active species that was considered to be a BH adduct. X-ray crystallographic analysis of one ESR-inactive product confirmed a singly-bonded derivative of $\text{La}@C_{2v}\text{-C}_{82}$ that corresponds to an oxidized BH intermediate formed at C23 position (see Scheme 1a). Moreover, when heated to 80 °C in anhydrous *o*-dichlorobenzene (*o*-DCB), all the synthesized singly-bonded products decompose to give the parent $\text{La}@C_{2v}\text{-C}_{82}$ as the major product. On the contrary, the BH product showed higher thermal stability. Based on the fact that a more positively charged carbon atom could be a more favored reaction site towards a nucleophilic attack, the authors proposed C18, C14, and C21 as the possible addition sites for the three unknown ESR-inactive products. The authors made their estimations based on Mulliken charge distribution analysis as determined by density functional theory (DFT) calculations.^[49]

We consider that the theoretical study of the BH addition to $\text{La}@C_{2v}\text{-C}_{82}$ is timely and relevant for three main reasons: i) because the relatively high abundance of $\text{La}@C_{82}$ among endohedral

monometallofullerenes makes the reactivity of this EMF one of the most studied (although not fully understood yet); ii) because of the radical character of the fullerene cage in La@C_{2v}-C₈₂, a non-conventional reaction mechanism for the BH addition to La@C_{2v}-C₈₂ can be expected (this is confirmed by the presence of singly-bonded derivatives in the observed products); and iii) because experiments were unable to definitely identify all adducts generated in the BH addition to La@C_{2v}-C₈₂. In this contribution, we have carried out an extensive quantum chemical (DFT) exploration of the various mechanistic pathways of the BH reaction between the anion dimethyl bromomalonate (**dmbm**⁻) and La@C_{2v}-C₈₂ through different reaction sites with two main objectives: i) to determine the reaction mechanism of the different reaction pathways; and ii) to evaluate the regioselectivity of the BH reaction of **dmbm**⁻ to La@C_{2v}-C₈₂ to provide a comprehensive description for the preference of different positions to react. For the particular case of the Diels-Alder reaction of (1,2,3,4,5-pentamethyl)cyclopentadiene to La@C_{2v}-C₈₂,^[51] some of us^[18] demonstrated by means of DFT calculations that this cycloaddition occurs regioselectively at bond **o** (shown in Scheme 1a) which corresponds to both, the thermodynamically and kinetically most favored attack, independently of the diene used for the reaction. We anticipate here that our results show that the BH reaction of **dmbm**⁻ to La@C_{2v}-C₈₂ is not as regioselective as the Diels-Alder reaction.

2. Computational Details

All DFT calculations were performed by using the Amsterdam Density Functional (ADF) program.^[52] An uncontracted set of Slater-type orbitals (STOs) of double- ζ (DZP) and triple- ζ (TZP) quality containing diffuse functions and one set of polarization functions were used to expand the molecular orbitals (MOs). The frozen-core approximation (FCA)^[52] was employed during the SCF procedure for the core orbitals of C, O, and La (*1s* for C and O and *1s2s2p3s3p4s3d4p* for La). It was shown that the FCA has a negligible effect on optimized geometries.^[53,54] Scalar relativistic corrections were included self-consistently by using the zeroth order regular approximation (ZORA).^[55]

The local density approximation (Slater exchange) with non-local corrections for exchange (Becke88)^[56] and correlation (Perdew86)^[57] (i.e. the BP86 functional) were used to self-consistently calculate energies and gradients. Although it is well documented that standard DFT functionals like BP86 underestimate energy barriers,^[58] this underestimation should be similar for all the BH transition states we encounter here and should not affect the main conclusions. Calculations were executed under the unrestricted formalism. Moreover, dispersion energy corrections as developed by Grimme *et al.*^[59,60] including the so-called Becke and Johnson damping (D3-BJ) were added in the calculation of DFT energies and gradients. It has been shown

that dispersion corrections are essential for a correct description of the thermodynamics and kinetics of reactions with fullerenes, nanotubes and other systems and reactions involving non-repulsive steric contact.^[61]

Geometry optimizations were performed without symmetry constraints in the gas phase. All stationary points were characterized by analytical frequency calculations. Electronic energies were obtained in solution with the TZP basis set by single-point energy calculations at the geometries optimized with the DZP basis (i.e. BP86-D3(BJ)/TZP//BP86-D3(BJ)/DZP). Solvent effects were introduced using the conductor-like screening model (COSMO)^[62] as implemented in ADF, performing single point energy calculations on the gas-phase optimized structures and using toluene as a solvent. In the Supporting Information (see Tables S1 and S2) we show that the gas-phase geometry is practically identical to the geometry optimized under the implicit presence of toluene.

In the search of minima and first-order saddle points the QUILD code (quantum regions interconnected by local descriptions)^[63] was used. QUILD works as a wrapper around the ADF program; it creates input files for ADF, then executes this program and collects energies and gradients. QUILD uses adapted delocalized coordinates and constructs model Hessians with the appropriate number of eigenvalues.^[64] This latter feature is particularly useful for the search of transition state structures.

Gibbs energies in solution (G_{tol}) were calculated from electronic energies at the (COSMO:Toluene)BP86-(BJ-D₃)/TZP//BP86-(BJ-D₃)/DZP level of theory—in toluene; corrections by zero-point energies, thermal contributions to the internal energy, and the entropy term were determined in the gas phase at the BP86-(BJ-D₃)/DZP level of theory using the statistical thermodynamics expressions of an ideal gas in standard conditions at 298 K. Lastly, to account for the condition change from 1 atm to 1 M concentration related to the phase change from gas to solution, we added to the G_{tol} values a concentration correction of 1.89 kcal/mol.^[65-67]

3. Results and Discussion

This section is divided as follows. Firstly, the 65 possible reaction pathways are defined to introduce the reader to the many different stationary points. Then, based on a complete thermodynamic study of the system, a classification of available energy profiles is performed so as to identify the thermodynamic products and, in turn, the potentially accessible kinetic products. Such a classification is designed with the purpose of predicting the experimentally observed products, either a singly-bonded or a cyclopropanated derivative. The kinetic study

therefore is conducted through all those reaction pathways that, in fact, lead to a cyclopropanated derivative prone to be experimentally observed.

3.1. General aspects of the 65 possible reaction pathways

In the initial step of the BH addition, a singly-bonded derivative is formed when **dmbm**[•] is attached to a specific carbon atom of La@C_{2v}-C₈₂. In the resulting structure, bromine is oriented toward an adjacent 6-MR or five-membered ring (5-MR) so that the reactive carbon atom of **dmbm**[•] faces the carbon atom of the cage that will be attacked (see Fig. 1). The rotation of the dihedral angle φ by $\pm 120^\circ$ in the resulting intermediate structure (φ is a structural parameter indicating the alignment between the bromine atom and a bond of the EMF cage; φ is equal to 0° or $\pm 180^\circ$ when bromine is exactly aligned with a [6,6] bond), generates three orientational isomers for each intermediate structure leading to different products. This is general, except when **dmbm**[•] is linked to carbon atoms C2, C3, C5, C8, C17, C20, and C24, in which only two orientational isomers can be distinguished because of the symmetry of the cage. Every single nonequivalent carbon atom represents one reaction site, and the formation of distinct orientational isomers of a singly-bonded derivative gives rise to 65 different reaction pathways, some of them leading to the same product (e.g., cyclopropanation to bond **1** can be achieved from either C1 or C2, see Scheme 1a).

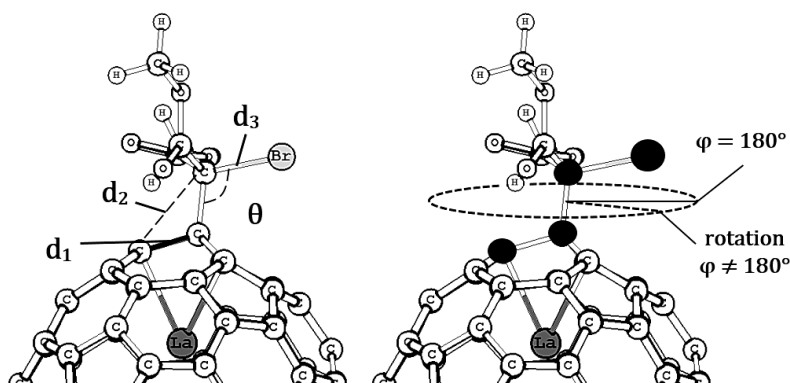
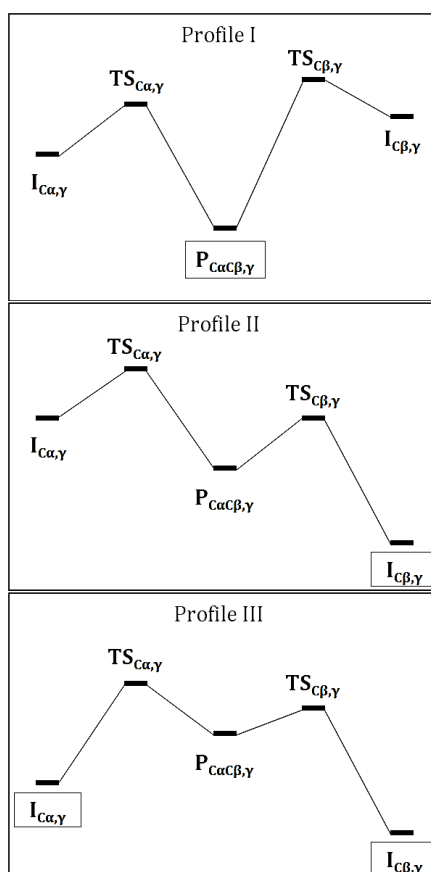


Figure 1. Structural parameters of a singly-bonded derivative. The distances d_n are geometrical descriptors of the cyclopropanation reaction happening at the bond highlighted in black (to the left). Angle θ and dihedral angle φ (this latter formed by the black-marked carbon atoms to the right) describe the position and orientation of the bromine atom (see text for details).

As mentioned in the introduction, it is well known that under typical conditions and in the case of EMFs, the BH reaction occurs under kinetic control.^[47,68] Therefore, a complete DFT-based study must be performed through the 65 different reaction pathways available in La@C_{2v}-C₈₂. However, it is important to keep in mind that there are two possible reaction pathways leading to **P**_{C α C β , γ (or ***P**_{C α C β , γ if the case). One of them follows the consecutive formations of **I**_{C α , γ and}}}

$\text{TS}_{\text{C}\alpha,\gamma}$; and analogously the other goes through $\text{I}_{\text{C}\beta,\gamma}$ and $\text{TS}_{\text{C}\beta,\gamma}$. In this regard, based on the energetic stability of $\text{I}_{\text{C}\alpha,\gamma}$, $\text{I}_{\text{C}\beta,\gamma}$, and $\text{P}_{\text{C}\alpha\text{C}\beta,\gamma}$ (or $^*\text{P}_{\text{C}\alpha\text{C}\beta,\gamma}$), in Scheme 2 we draw a picture with the intention of representing the three situations susceptible to occur. Observe that profile type I is defined as the energy profile in which both reaction pathways lead to a Bingel product that is more stable than the two possible intermediate precursors ($\text{I}_{\text{C}\alpha,\gamma}$ and $\text{I}_{\text{C}\beta,\gamma}$). If one reaction pathway could be reverted, then profile type II is defined, where the BH product is more stable than only one of the intermediate precursors. Finally, profile type III corresponds to the energy profile involving a destabilized Bingel product with respect to $\text{I}_{\text{C}\alpha,\gamma}$ and $\text{I}_{\text{C}\beta,\gamma}$. For profiles II and III we expect that the corresponding BH retro-reaction will happen and the BH product will not be accumulated. Accordingly, the following subsections are conducted regarding the profile classification of the 65 reaction pathways with the aim of describing all the most thermodynamically and kinetically favored BH reactions.

Scheme 2. Representation of the two reaction pathways leading to the formation of a Bingel-Hirsch adduct as a fulleroid or a methanofullerene through the attack on bond γ with adjacent reaction centers $\text{C}\alpha$ and $\text{C}\beta$. The energy profile in which the retro-Bingel-Hirsch addition is hampered is classified as profile type I. On the contrary, if one or two reaction pathways can be regressed to a singly-bonded derivative then the resulting profiles are respectively classified as II or III. For every diagram, the most likely structure to be experimentally accumulated is enclosed in a rectangular box.



3.2. Classification of the 65 possible reaction pathways

Gibbs energies in toluene (ΔG_{tol}) relative to separated reactants for the formation of the 65 different $\mathbf{I}_{C\alpha,\gamma}$ structures are reported in Table 1, as well as ΔG_{tol} for the 35 most stable BH adducts (mostly $\mathbf{P}_{C\alpha C\beta,\gamma}$ adducts). Based on Scheme 2 and the values of ΔG_{tol} for the structures related to a single pathway, it is possible to define the profile type in which that reaction pathway can be classified (e.g. for the attack on bond **1**, $\mathbf{P}_{C1C2,1}$ is more stabilized than $\mathbf{I}_{C1,1}$ and $\mathbf{I}_{C2,1}$; therefore the situation is described by profile type I). After analyzing the profile type for all the 65 available reaction pathways, as reported in Table 1, we find that only 15 attacks out of 35 are of profile type I. These 15 attacks can occur through 26 different pathways ($C\alpha = C\beta$ for bonds **9**, **16**, **18**, and **a**) and generate relatively stable BH products. To determine the kinetics of the entire BH addition to $\text{La}@C_{2v}\text{-C}_{82}$, we focus on reaction pathways with profile type I because only in this situation the BH adduct is going to be experimentally observed. Furthermore, in principle the 65 different intermediates $\mathbf{I}_{C\alpha,\gamma}$ must be completely characterized. However, in a few cases exhibiting type II and III profiles, we did not optimize all possible orientational isomers of intermediate $\mathbf{I}_{C\alpha,\gamma}$ as they exhibit similar energetics (see superscript *a* in Table 1). To sum up, by strategically defining three different profiles of the BH addition to $\text{La}@C_{2v}\text{-C}_{82}$ based on ΔG_{tol} of all the possible intermediates, methanofullerenes, and fulleroids, we can avoid the study of a number of reaction pathways and still provide a full description of this reaction; therefore in the following subsection the kinetic study is described for the 26 reaction pathways related to profile type I.

Table 1. Classification according to Scheme 2 based on energetic stability (in kcal/mol) of $\mathbf{I}_{\text{C}\alpha,\gamma}$, $\mathbf{I}_{\text{C}\beta,\gamma}$, and $\mathbf{P}_{\text{C}\alpha\text{C}\beta,\gamma}$, of all possible Gibbs energy profiles for the Bingel-Hirsch addition to $\text{La}@C_{2v}\text{-C}_{82}$ in toluene. The structural classification (see Scheme 1a) of bond γ is also given. Marked in italics the most stable intermediates (criterion: $\Delta G_{\text{tol}} < -10.0$ kcal/mol).

γ	Bond type	C α	C β	ΔG_{tol}			Profile
				$\mathbf{I}_{\text{C}\alpha,\gamma}$	$\mathbf{I}_{\text{C}\beta,\gamma}$	$\mathbf{P}_{\text{C}\alpha\text{C}\beta,\gamma}$	
1	B	1	2	-7.82	-13.49	-15.40	I
2	B	6	7	-8.15 ^a	-10.38	-9.71	II
3	B	4	7	-8.78	-10.86	-12.37	I
4	B	7	10	-8.96	-8.03 ^a	-7.96 ^b	III
5	B	5	8	-3.58 ^a	-7.81 ^a	-2.89	III
6	B	9	12	-5.67 ^a	-7.40	-0.48	III
7	B	12	13	-7.84	-10.59	-12.39	I
8	B	8	11	-7.81	-11.54	-6.03	III
9	C	15	15	0.69	0.69	-15.93	I
10	C	12	15	-7.91	2.18	-11.97	I
11	B	15	18	-0.15	-9.46	-15.40	I
12	A	16	19	-3.59 ^a	-11.16	-9.93 ^b	II
13	B	14	17	-8.05	-6.44	-10.66	I
14	C	17	20	-6.99	3.87	-16.56	I
15	B	20	21	5.09	-10.88	-9.56	II
16	A	22	22	-6.48	-6.48	-10.09 ^b	I
17	B	23	24	-13.46	1.92	-7.86	II
18	C	24	24	2.42	2.42	-18.04	I
19	B	2	3	-14.92	-7.63	-18.52	I
a	D	1	1	-7.76	-7.76	-15.58	I
b	D	18	22	-11.28	-6.48 ^a	-4.49	III
c	D	3	6	-8.09	-7.81	-7.27	III
d	D	1	4	-7.82 ^a	-9.47	-8.79	II
e	D	4	5	-9.58	-3.58	-9.45	II
f	D	6	9	-8.15	-5.67	-12.42	I
g	D	9	9	-5.67 ^a	-5.67 ^a	2.10 ^b	III
h	D	10	13	-7.23	-10.73	-10.77	I
i	D	10	11	-8.03	-10.40	-12.71	I
j	D	11	14	-11.55	-9.09	-9.26	II
k	D	14	16	-9.11	-3.59	-0.29	III
l	D	13	16	-11.30	-3.59 ^a	-4.93	II
m	D	18	19	-10.28	-10.58	-7.23	III
n	D	19	21	-11.68	-10.49	-9.86	III
o	D	21	23	-11.14	-13.74	-10.30	III
p	D	22	23	-4.63	-12.37	-8.87	II

^a ΔG_{tol} for these intermediates was estimated from the energy of the most stable orientational isomer for that specific reaction site. For instance, the energy of $\mathbf{I}_{\text{C}9,6}$ is not calculated, but it is taken as the energy of $\mathbf{I}_{\text{C}9,f}$ since orientational isomers are energetically very similar. Moreover, from the energy of $\mathbf{I}_{\text{C}12,6}$ it is possible to anticipate that bond **6** is not indeed involved in a profile type I.

^b Only in these four cases, $^*\mathbf{P}_{\text{C}7\text{C}10,4}$, $^*\mathbf{P}_{\text{C}9\text{C}9,g}$, $^*\mathbf{P}_{\text{C}16\text{C}19,12}$, and $^*\mathbf{P}_{\text{C}22\text{C}22,16}$, the most stable Bingel-Hirsch adduct is a methanofullerene instead of a fulleroid structure.

3.3. Analysis of structural parameters through the reaction coordinate

Relevant structural parameters (d_1 , d_2 , d_3 , θ , and φ as defined in Figure 1) are summarized in Table 2 for the 26 reaction pathways under consideration. The distance d_1 describes the bond length of the attacked C–C bond γ of the cage, d_2 corresponds to the C_{C82} – C_{dmbm} that is formed during the ring closure, and d_3 refers to the C_{dmbm} – C_{Br} bond length. The angles θ and φ are useful parameters for the examination of the exact localization of bromine through the reaction coordinate. In addition to that, from the reaction sites $C\alpha$ involved in those 26 reaction pathways, there are seven 666 positions (carbon atoms surrounded by three hexagons) and eleven 566 (carbon atoms surrounded by one pentagon and two hexagons) that lead to eleven [6,6] and four [5,6] BH adducts (one bond is type A, six type B, four type C, and four type D). Therefore, there are fifteen potential $P_{C\alpha C\beta, \gamma}$ (or $*P_{C\alpha C\beta, \gamma}$ if more stable) structures to be observed.

The structural parameter d_1 remains constant through the different $I_{C\alpha, \gamma}$ and $TS_{C\alpha, \gamma}$ structures under study. However, for the cyclopropanated adduct $d_1 > 2.0$ Å indicating the rupture of the attacked C–C bond γ in the cage (except for $*P_{C22C22,16}$, for which it was not even possible to optimize the analogous open-cage structure $P_{C22C22,16}$). On the other hand, the structural parameter d_2 starts in $I_{C\alpha, \gamma}$ at ca. 2.6 Å and is shortened to 1.8-1.9 Å at $TS_{C\alpha, \gamma}$; then d_2 acquires the characteristic value of a hybridized $C(sp^3)$ – $C(sp^2)$ bond length when $P_{C\alpha C\beta, \gamma}$ is formed (i.e. ~ 1.48 Å), thus confirming the ring closure.

The other parameters, d_3 , θ , and φ , account for the position of bromine through the reaction coordinate. The bond length d_3 between bromine and the reactive carbon atom of $dmbm\cdot$ is ca. 2.0 Å for the initial structure $I_{C\alpha, \gamma}$; and it is elongated by 0.7-0.9 Å while d_2 is simultaneously shortened to reach the transition state structure in a S_N2 -like process. In the final product, bromine is completely dissociated as bromide, $d_3 \rightarrow \infty$. Moreover, the reactive carbon atom of $dmbm\cdot$ has a tetrahedral arrangement in every $I_{C\alpha, \gamma}$ structure since θ is nearly 109.5°. When $TS_{C\alpha, \gamma}$ is reached, θ is decreased to 90° as the reaction evolves toward the ring closure. On the other hand, we observe that $I_{C\alpha, \gamma}$, $I_{C\alpha, \delta}$, and $I_{C\alpha, \varepsilon}$ (the latter if available) formed at the center $C\alpha$ are structurally very similar and they differ only in their dihedral angle φ . If $C\alpha$ is a 566 center then bromine can be oriented $\pm 180^\circ$ with respect to a [6,6] bond γ , and the other [5,6] bonds δ or ε result in $\varphi \approx \pm 180^\circ \pm 120^\circ \approx \pm 60^\circ$ (see for instance φ for intermediates at C1 in Table 2). In the case of a 666 center, we selected the bond having the label with the smallest number as the reference point (e.g. in Table 2, for $I_{C15,9}$ $\varphi \approx \pm 180^\circ$ and the others, $I_{C15,10}$ and $I_{C15,11}$, have $\varphi \approx \pm 60^\circ$).

Table 2. Structural parameters (in Å, deg.) and Gibbs energies in toluene ΔG_{tol} (in kcal/mol) relative to separated reactants of key stationary points in the explored Bingel-Hirsch reaction pathways.^a

C α	γ	Intermediate (I _{Cα,γ})						Transition State (TS _{Cα,γ})						Product (P _{CαCβ,γ})		
		d ₁	d ₂	d ₃	θ	φ^b	ΔG_{tol}	d ₁	d ₂	d ₃	θ	φ^b	$\Delta G_{\text{tol}}^\ddagger$	d ₁	d ₂	ΔG_{tol}
C1	1	1.520	2.552	2.004	108.8	-172.7	-7.82	1.538	1.799	2.844	89.5	179.0	13.71	2.134	1.484	-15.40
C1	a	1.544	2.597	1.998	107.9	53.7	-7.76	1.556	1.825	2.825	88.6	60.2	16.58	2.168	1.486	-15.58
C2	1	1.540	2.588	1.995	107.6	178.0	-13.49	1.562	1.825	2.745	92.5	-179.6	13.13	2.134	1.484	-15.40
C2	19	1.541	2.596	1.995	107.5	54.9	-14.92	1.561	1.888	2.764	89.4	63.2	15.75	2.154	1.481	-18.52
C3	19	1.532	2.562	2.003	108.8	-173.0	-7.63	1.539	1.855	2.796	90.0	176.7	6.29	2.154	1.481	-18.52
C4	3	1.520	2.559	2.003	108.5	-175.2	-8.78	1.542	1.806	2.847	88.6	178.2	14.25	2.157	1.481	-12.37
C6	f	1.552	2.593	2.006	108.0	53.5	-8.15	1.543	1.919	2.836	84.8	56.6	9.41	2.187	1.484	-12.42
C7	3	1.539	2.591	1.994	107.3	57.5	-10.86	1.628	1.842	2.708	93.1	75.7	16.20	2.157	1.481	-12.37
C9	f	1.545	2.583	2.000	108.2	-64.9	-5.67	1.543	1.877	2.748	89.4	-72.2	9.49	2.187	1.484	-12.42
C10	h	1.550	2.586	2.006	108.0	-63.2	-7.23	1.545	1.855	2.813	86.1	-69.2	9.13	2.187	1.488	-10.77
C10	i	1.551	2.593	1.998	107.7	54.5	-8.03	c	c	c	c	c	13.26 ^c	2.233	1.488	-12.71
C11	i	1.549	2.617	1.985	108.7	-42.4	-10.40	1.544	1.847	2.799	89.1	-58.2	15.74	2.233	1.488	-12.71
C12	7	1.525	2.578	2.002	108.1	55.4	-7.84	1.546	1.905	2.755	88.0	71.3	11.90	2.208	1.475	-12.39
C12	10	1.580	2.601	2.001	107.2	-69.3	-7.91	1.597	1.859	2.861	86.4	-76.8	17.16	2.284	1.489	-11.97
C13	7	1.531	2.575	2.007	107.8	-175.8	-10.59	1.547	1.934	2.888	82.6	172.8	10.50	2.208	1.475	-12.39
C13	h	1.539	2.593	1.999	108.0	52.3	-10.73	1.538	1.928	2.834	84.7	49.1	15.96	2.187	1.488	-10.77
C14	13	1.542	2.600	1.993	109.8	-158.7	-8.05	1.544	1.882	2.852	85.6	-170.5	9.82	2.192	1.493	-10.66
C15	9	1.577	2.573	2.004	108.2	177.0	0.69	1.593	1.859	2.785	89.4	175.3	13.21	2.318	1.492	-15.93
C15	10	1.562	2.567	2.001	108.2	59.4	2.18	1.574	1.853	2.795	89.6	70.2	13.59	2.284	1.489	-11.97
C15	11	1.539	2.562	2.010	109.7	-68.6	-0.15	1.551	1.901	2.700	90.9	-76.7	5.72	2.231	1.497	-15.40
C17	13	1.527	2.576	2.001	108.3	-179.7	-6.44 ^d	1.548	1.889	2.723	90.4	-176.3	17.89	2.192	1.493	-10.66
C17	14	1.586	2.593	2.001	107.3	-58.0	-6.99 ^d	c	c	c	c	c	20.58 ^c	2.305	1.495	-16.56
C18	11	1.551	2.575	2.012	108.0	178.6	-9.46	1.554	1.972	2.921	80.6	161.2	9.76	2.231	1.497	-15.40
C20	14	1.575	2.574	2.004	107.8	-175.8	3.87	1.618	1.912	2.839	85.3	-176.4	17.47	2.305	1.495	-16.56
C22	16	1.479	2.535	1.991	110.9	174.2	-6.48	1.481	1.908	2.755	92.9	-175.1	6.75	1.517	1.512	-10.09 ^e
C24	18	1.577	2.602	1.990	108.4	-70.8	2.42	1.624	1.945	2.840	84.0	-82.9	18.13	2.311	1.493	-18.04

^a Structural parameters defined in Figure 1. $\Delta G_{\text{tol}}^\ddagger$ (kcal/mol) is the Gibbs energy barrier in toluene for the ring-closure step; this is estimated as the energy difference between **TS**_{C α , γ} and **I**_{C α , γ} if the intermediate is more stable than separated reactants; otherwise it is the energy difference between **TS**_{C α , γ} and separated reactants. All reaction pathways are of profile type I as explained in Scheme 2.

^b For the dihedral angle φ , if C α is a 566 center then bromine can be oriented $\pm 180^\circ$ with respect to a [6,6] bond γ , and the other [5,6] bonds result in $\varphi \approx \pm 180^\circ \pm 120^\circ \approx \pm 60^\circ$. On the other hand, if C α is a 666 center, we select the bond having the label with the smallest number as the reference point (e.g., for **I**_{C15,9} $\varphi \approx \pm 180^\circ$ and the others, **I**_{C15,10} and **I**_{C15,11}, have $\varphi \approx \pm 60^\circ$).

^c See Figure S1 in the Supporting Information for the discussion of the transition states for these reaction pathways. $\Delta G_{\text{tol}}^\ddagger$ values are estimated from linear transits.

^d See Figures S2 and S3 in the Supporting Information for a discussion of the movement of the La atom in these structures.

^e Only in the case of ***P**_{C22C22,16} the most stable Bingel-Hirsch adduct is a methanofullerene instead of a fulleroid structure.

3.4. Fullerooids vs methanofullerenes

We have studied the relative stability of open-cage/closed-cage (fulleroid/methanofullerene) monoadducts. In all cases in which it was possible to optimize both the closed- and open-cage adducts, the fulleroid structure was found to be more stable than the methanofullerene adduct; except for the case of $*\mathbf{P}_{\mathbf{C}9\mathbf{C}9,\mathbf{g}}$. In general, one may optimize both structures but the fulleroid is usually the most stable (see Table S3 in the Supporting Information for a complete analysis of all optimized closed- and open-cage BH adducts).^[68] In the cases of $*\mathbf{P}_{\mathbf{C}7\mathbf{C}10,4}$, $*\mathbf{P}_{\mathbf{C}16\mathbf{C}19,12}$, and $*\mathbf{P}_{\mathbf{C}22\mathbf{C}22,16}$, we were not able to optimize an open-cage adduct and only the methanofullerene BH adducts were located. The reaction barrier for the conversion of the cyclopropanated adduct to the fulleroid structure is found to be around 1 kcal/mol. To illustrate this point, Figure 2 depicts the gas-phase linear transit from methanofullerenes $*\mathbf{P}_{\mathbf{C}1\mathbf{C}2,1}$ and $*\mathbf{P}_{\mathbf{C}21\mathbf{C}23,0}$ to fulleroids $\mathbf{P}_{\mathbf{C}1\mathbf{C}2,1}$ and $\mathbf{P}_{\mathbf{C}21\mathbf{C}23,0}$, respectively. For the former, the fulleroid is the most stable while, in the latter, the cyclopropanated structure is marginally more stable than the analogous fulleroid in the gas phase but not in solution. Solvent effects stabilize open-cage adducts more than closed-cage ones (see Table S3).

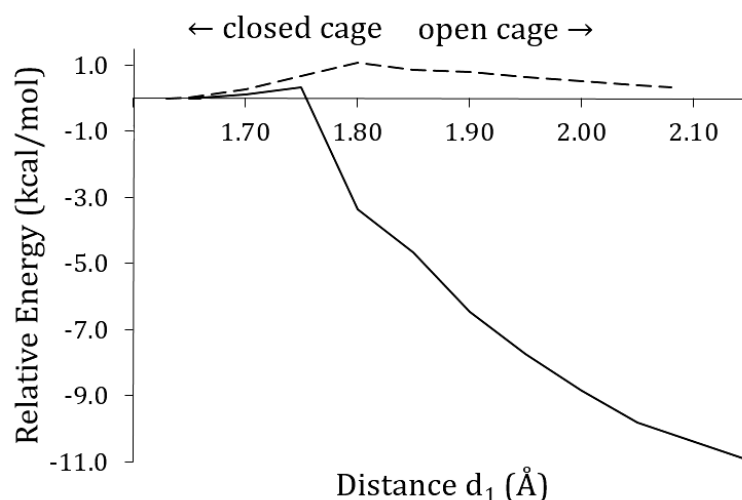


Figure 2. Gas-phase linear transit for rupture of bonds **1** in $*\mathbf{P}_{\mathbf{C}1\mathbf{C}2,1}$ (solid line) and **o** in $*\mathbf{P}_{\mathbf{C}21\mathbf{C}23,0}$ (dashed line). Initial (left) and final (right) points respectively correspond to the closed- and open-cages at their optimized geometries. Energies (kcal/mol) are relative to the gas-phase optimized closed-cage adduct at the BP86-D3(BJ)/DZP level of theory.

To discuss the origin of the higher stability of the open-cage adducts we performed an activation strain analysis (ASM)^[69–71] of the reactivity (also known as the distortion/interaction model)^[72–74] along the reaction pathways leading to the open-cage $\mathbf{P}_{\mathbf{C}1\mathbf{C}2,19}$ (see Figure 3). In the ASM analysis, the relative energy with respect to separated reactants, ΔE , along the reaction coordinate

is decomposed into the strain ΔE_{strain} associated with deforming the individual reactants and the actual interaction ΔE_{int} between the deformed reactants:

$$\Delta E = \Delta E_{strain} + \Delta E_{int}$$

The open-cage structure $\mathbf{P}_{C1C2,19}$ is found to be more distorted by 33.2 kcal/mol in terms of ΔE_{strain} than the $^*\mathbf{P}_{C1C2,19}$ closed one. This large structural deformation in the open-cage structure is compensated by the interaction term, ΔE_{int} , which is 43.6 kcal/mol more stabilizing than the interaction in its corresponding closed-cage adduct. The resulting binding energy given as $\Delta E_{def} + \Delta E_{int}$ shows that the open-cage $\mathbf{P}_{C1C2,19}$ is more stabilized by 10.4 kcal/mol as compared to the closed-cage one. The reason for the ΔE_{int} term being more stabilizing in the open cage is twofold. First, the breaking of the attacked C–C bond in the fullerene cage stabilizes the LUMO and destabilizes the HOMO of the carbon cage, making frontier orbitals interactions more favorable.^[75] Moreover, in open-cage adducts all carbon atoms keep their sp^2 hybridization forming homoaromatic rings, maintaining their π -delocalization. This π -homoconjugation has been shown to be crucial for the final stabilization of open-cage EMFs BH adducts.^[19,46] In addition, we have applied the ASM analysis to other reaction pathways and, in all cases, we arrive at the same conclusion that, regardless the higher structural distortion, the open-cage adduct tends to be more stabilized than the closed-cage one because of the higher interaction between the reactants (see Table S4 in the Supporting Information).

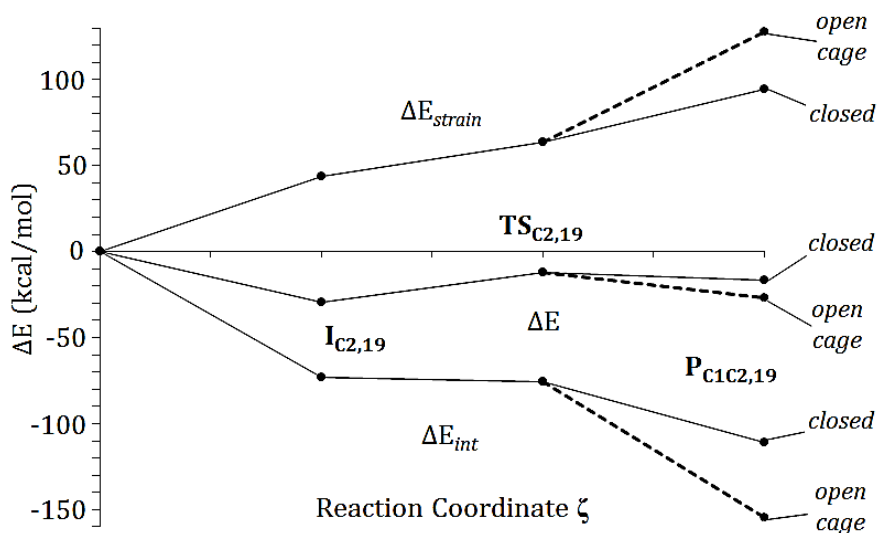


Figure 3. Activation strain diagram for the Bingel-Hirsch pathway at bond **19** between C1 and C2 (dashed line = path to open-cage $\mathbf{P}_{C1C2,19}$; solid line = path to closed-cage $^*\mathbf{P}_{C1C2,19}$).

3.5. The most favored reaction pathways

We were able to optimize 24 $\text{TS}_{\text{Ca},\gamma}$ out of the 26 possible transition states of reaction pathways with profile type I. In Figure S1 in the Supporting Information, linear transit calculations of the two missing $\text{TS}_{\text{Ca},\gamma}$ structures show that they are very high in energy. From the experimental evidence provided by Nagase *et al.*,^[20,49] five different structures were isolated revealing the following product distribution (in percentage): 55.4, 22.1, 5.5, 5.1, and 11.9. From the reaction energies ΔG_{tol} reported in Table 1, we have determined that the most stable intermediate is generated at the C2 position with the orientational isomer $\text{I}_{\text{C}2,19}$ very close in energy to $\text{I}_{\text{C}23,6}$ by 1.2 kcal/mol. The orientational isomers of $\text{I}_{\text{C}2}$ and $\text{I}_{\text{C}23}$ are connected to the corresponding addition products via relatively high energy transition states. Indeed, $\text{TS}_{\text{C}2,1}$, $\text{TS}_{\text{C}2,19}$, $\text{TS}_{\text{C}23,17}$, $\text{TS}_{\text{C}23,6}$, and $\text{TS}_{\text{C}23,\text{p}}$ are associated with energy barriers of 13.1, 15.8, 13.5, 21.5 and 15.2 kcal/mol, respectively (the three latter barriers are not shown in Table 2 because they were not classified into profile type I; however, they are reported in Table S5 in the Supporting Information). Those activation energies are not in competition with the lowest ones, which are calculated for $\text{TS}_{\text{C}15,11}$ and $\text{TS}_{\text{C}3,19}$ to be 5.7 and 6.3 kcal/mol (see Figure 4), respectively. Nonetheless, $\text{I}_{\text{C}15,11}$ and $\text{I}_{\text{C}3,19}$ are relatively destabilized as compared to $\text{I}_{\text{C}2,19}$ by respectively 14.8 and 7.3 kcal/mol. In fact, if formed, $\text{I}_{\text{C}15,11}$ would likely decompose into reactants since the process leading to the formation of this intermediate is certainly not favored ($\Delta G_{\text{tol}} = -0.2$ kcal/mol). A similar statement was given by Zhao *et al.* in a very recent study of the BH addition to the non-IPR $\text{Sc}_2@\text{C}_{66}$; wherein reaction pathways with the lowest-energy barriers but destabilized intermediates were discarded to produce the experimentally observed BH adduct.^[68] Based on these results we conclude that the most favored reaction pathway leads to the formation of a fulleroid derivative on bond **19** rather than on bond **11** (although the formation of this latter cannot be totally discarded). These results are in agreement with the experimental evidence since only one of the five characterized structures corresponds to a BH product (**P**). In fact, from the ^{13}C NMR spectrum of anion **P**, and on the basis of the similar NMR spectra of previously reported cycloadditions leading to open-cage adducts,^[19,49] the authors concluded that the observed signals correspond to sp^2 carbon atoms of an open-cage adduct attacked at a [6,6] position. For instance, in the case of the formation of the $\text{Y}_3\text{N}@\text{C}_{80}$ fulleroid, X-ray analysis confirmed the formation of an open-cage monoadduct on a [6,6] bond.^[39] Moreover, based on NMR and UV spectra and DFT calculations, a [6,6] bond was suggested to be the attacked site for the formation of $\text{Sc}_3\text{N}@\text{C}_{80}$ BH derivative.^[76] We conclude, therefore, that the isolated $\text{La}@\text{C}_{2\nu}\text{-C}_{82}$ monoadduct structure corresponds to $\text{P}_{\text{C}2\text{C}3,19}$, a fulleroid formed on a [6,6] bond. There is also another competitive reaction pathway leading to $^*\text{P}_{\text{C}22\text{C}22,16}$, a methanofullerene, for which the respective energy barrier is only 0.5 kcal/mol higher than the one for the formation of

PC₂C_{3,19} (see Figure 4). Nevertheless, the formation of a BH product on bond **16** is discarded because the obtained closed-cage monoadduct is not in agreement with the experimentally observed fulleroid structure. It is interesting to notice that additions with the lowest energy barriers produce well-stabilized fulleroids. Indeed the most stable fulleroid is **P**C₂C_{3,19}. The great stability of **P**C₂C_{3,19} is in line with the experimental higher stability of the fulleroid as compared to the singly-bonded derivatives when heated at 80 °C.^[49]

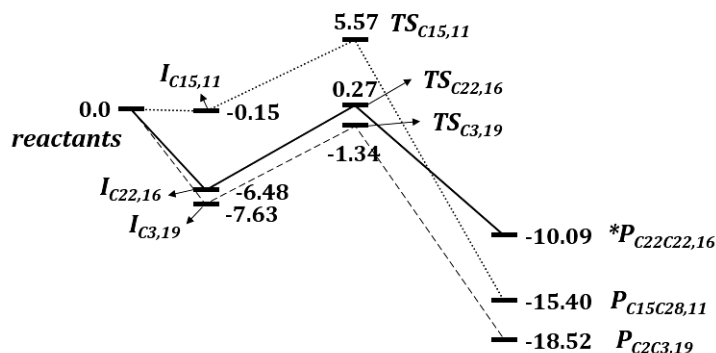


Figure 4. Comparison of the Gibbs energy profiles (in kcal/mol) for the lowest-barrier pathways to addition at C15 on bond **11** (dotted line), C3 on bond **19** (dashed-line), and C22 on bond **16** (solid line).

Three [6,6] bonds are determined to be the most reactive for the formation of the final BH adduct: **11** (type B), **16** (type A), and **19** (type B). For **16** and **19**, the initial intermediate formation occurs on a 566 carbon atom (C3 and C22), and for **11** at a 666 carbon atom (C15). The closure and final BH product formation takes place always on a [6,6] bond. The attack to bonds of type C (or *pyrene*), which only involve 666 carbons, results in relatively high energy barriers. Additionally, all the reaction pathways on *pyrene* bonds are classified with profile type I. Type D (or *corannulene*) bonds can be considered relatively unreactive since many reaction pathways happening on *corannulene* positions exhibit type II and III energy profiles, and those additions with profile I involving type D bonds have energy barriers higher than 10 kcal/mol. In general, we observe that the ring-closure between **dmbm**[•] and a [6,6] bond during the second step of the BH reaction is favored when a 5-MR is adjacent to the initially functionalized carbon atom, as shown for bond types A and B. Interestingly, bonds **11**, **16**, and **19** are among the ten most reactive bonds for the Diels-Alder cycloaddition to La@C_{2v}-C₈₂, but they are less reactive than bond **o**, which is the most reactive in this type of reactions.^[18]

Based on the ESR, NMR, and X-ray analysis carried out by Nagase *et al.*,^[49] four adducts were assigned to be singly-bonded derivatives. Those structures should correspond to the thermodynamically most stable intermediates: 666 positions C2 and C7 and 566 carbons C11, C13, C18, C19, C21, and C23 (see Table 1). The reaction pathways involving the intermediates formed at C23 are classified into profiles II or III: intermediates **I_{C23,17}**, **I_{C23,o}**, and **I_{C23,p}** are at least 3 kcal/mol more stable than the corresponding fullerenes **P_{C23C24,17}**, **P_{C21C23,o}**, and **P_{C22C23,p}**. In addition, their formation is associated with activation energies twice or three times larger than the lowest ones (see Table S5). Consequently, we can conclude that the formation of the three products involving the formation of a C23 intermediate are kinetically hampered, resulting in an accumulation of the intermediate **I_{C23}** as the major product instead of the cyclopropanated derivative. This is in good agreement with the experimental observations since **I_{C23}** was the only structure confirmed by X-ray and had the highest yield (55.4%). The other structure with the second highest yield (22.1%) is also a singly-bonded derivative. We assign this structure to be **I_{C2}** because it is actually the thermodynamically most stable singly-bonded structure (1.2 kcal/mol below the energy of **I_{C23}**), and the reaction pathways through the bonds around C2 are associated with activation energies higher than 13 kcal/mol. In view of that, one might expect the same yield for **I_{C2}** and **I_{C23}**. Nonetheless, unlike C23, reaction pathways around C2 do actually produce well-stabilized fullerenes and are classified as type I. In fact the most stable structure is **P_{C2C3,19}**. Consequently, a portion of **I_{C2}** may be consumed to produce **P_{C2C3,19}** during the BH reaction, thus being the second most abundant singly-bonded adduct.

Table 3. VDD atomic charges and spin densities ρ (both in a.u.) for selected carbon atoms in the La@C_{2v}-C₈₂ cage.^a

Cα	VDD	ρ
C2	-0.01	0.02
C3	-0.01	0.02
C11	-0.01	0.00
C13	-0.01	-0.01
C15	0.00	0.02
C18	-0.01	0.04
C19	-0.01	0.03
C21	0.00	-0.01
C22	-0.01	-0.01
C23	0.00	0.05

^a Computed at BP86-D3(BJ)/DZP level of theory.

The remaining two experimentally-characterized singly-bonded derivatives with a product distribution of 5% each, should correspond to the other well-stabilized intermediates, which are formed at C7, C11, C13, C18, C19, and C21 positions. Based on our computations, we predict that the **I_{C19}** and **I_{C21}** structures are the ones experimentally detected because they are thermodynamically stable (after C2 and C23, the lowest-energy intermediate is generated at C19) and all the BH products coming from C19 and C21 intermediates are non-stable fulleroids (i.e. their reaction pathways are classified into profiles II or III, just like C23). However, the formation of singly-bonded derivatives on C7, C11, C13, C18 positions cannot be fully discarded. Consequently, our results show that La@C_{2v}-C₈₂ is not particularly regioselective under Bingel-Hirsch conditions. As a final remark, let us mention that we did not find any correlation between the predicted adducts and the position of the La atom in the La@C_{2v}-C₈₂ cage in terms of Voronoi-deformation-density (VDD) charge distribution^[77] and spin density, as reported in Table 3. These results are actually highlighting that these quantities cannot be used to make predictions about possible BH reaction sites.

4. Conclusions

We have quantum chemically identified the five experimentally observed but hitherto uncharacterized products in the Bingel-Hirsch (BH) addition of dimethyl bromomalonate to the $\text{La}@C_{2v}\text{-C}_{82}$. Only one of the experimentally observed products is a fulleroid. Our computations indicate that this is the fulleroid at bond **19** which emerges as the kinetically and thermodynamically most favorable Bingel-Hirsch adduct; however, our analysis made through all possible cyclopropanated derivatives suggests that the fulleroid on bond **11** cannot be totally discarded.

Based on experimental results by Nagase *et al.*,^[49] four adducts can be assigned to be singly-bonded derivatives. We assign two of the observed products with the highest yields to the thermodynamically most stable intermediates, **Ic2** and **Ic23**. According to our computations, these intermediates are traps on the Bingel-Hirsch reaction pathways. Formation of the final Bingel-Hirsch adduct is kinetically hampered leading to accumulation of these intermediates, especially in the case of **Ic23**. Likewise, the remaining two experimentally reported singly-bonded derivatives with a reduced product distribution are most likely **Ic19** and **Ic21**. Note, however, that the other well-stabilized intermediates formed at C7, C11, C13, and C18 may be in direct competition.

Finally, our computational exploration also shows that the Bingel-Hirsch addition to $\text{La}@C_{2v}\text{-C}_{82}$ is not particularly regioselective. It differs in this respect from the Diels-Alder cycloaddition that occurs exclusively at bond **o**. Thus, in the case of the Bingel-Hirsch reaction one may anticipate the formation of at least 10 products even under relatively mild reaction conditions.

Acknowledgements

We thank the following organizations for financial support: the Spanish government (MINECO, project numbers CTQ2014-54306-P and CTQ2014-59212-P), the Generalitat de Catalunya (project number 2014SGR931 and Xarxa de Referència en Química Teòrica i Computacional), and the FEDER fund (European Fund for Regional Development) for the grant UNGI10-4E-801. We thank the National Research School Combination - Catalysis (NRSC-C), and The Netherlands Organization for Scientific Research (NWO/CW and NWO/EW). J.P.M. gratefully acknowledges a Ph.D. fellowship (register/application no. 217067/312543) from the Mexican National Council of Science and Technology (CONACYT). M.G.-B. thanks the Spanish MEC for a doctoral fellowship no. AP2010-2517. S.O. thanks the MINECO for the Juan de la Cierva fellowship and the European Community for the CIG project (FP7-PEOPLE-2013-CIG-630978).

The authors are also grateful for the computer resources, technical expertise, and assistance provided by the HPC centers Barcelona Supercomputing Center - Centro Nacional de Supercomputación, SURFsara in Amsterdam, and the Centre de Serveis Científics i Acadèmics de Catalunya (CESCA). Support for the research of M.S. was received through the ICREA Academia 2014 prize for excellence in research funded by the Generalitat de Catalunya.

Supporting Information

A comparison between transition state geometries optimized in the gas phase and under solvent environment is shown in Tables S1 and S2. Figure S1 contains linear transit calculations for the two missing transition state structures; that is **TS_{C10,i}** and **TS_{C17,14}**. Figures S2 and S3 are related to the discussion about the movement of the La atom in the La@C_{2v}-C₈₂ cage for intermediates **Ic_{2,19}**, **Ic_{3,19}**, **Ic_{15,11}**, **Ic_{23,0}**, **Ic_{17,13}**, and **Ic_{17,14}**. In Table S3 the energies of methanofullerenes and fulleroids are compared. Table S4 reports the activation strain model for some selected reaction pathways. In Table S5 the structural parameters and Gibbs energy barriers in toluene are gathered for some selected reaction pathways classified into profile type II or III. Table S6 contains the absolute energies for all the structures under study (from reactants to products). Table S7 contains the Cartesian coordinates for all the 141 DFT-optimized structures located in this work.

5. References

- [1] J. R. Heath, S. C. O'Brien, Q. Zhang, Y. Liu, R. F. Curl, F. K. Tittel, R. E. Smalley, *J. Am. Chem. Soc.* **1985**, *107*, 7779–7780.
- [2] X. Lu, L. Feng, T. Akasaka, S. Nagase, *Chem. Soc. Rev.* **2012**, *41*, 7723–7760.
- [3] M. N. Chaur, F. Melin, A. L. Ortiz, L. Echegoyen, *Angew. Chem. Int. Ed.* **2009**, *48*, 7514–7538.
- [4] S. Yang, F. Liu, C. Chen, M. Jiao, T. Wei, *Chem. Commun.* **2011**, *47*, 11822–11839.
- [5] A. A. Popov, S. Yang, L. Dunsch, *Chem. Rev.* **2013**, *113*, 5989–6113.
- [6] X. Lu, L. Bao, T. Akasaka, S. Nagase, *Chem. Commun.* **2014**, *50*, 14701–14715.

- [7] H. Cong, B. Yu, T. Akasaka, X. Lu, *Coord. Chem. Rev.* **2013**, *257*, 2880–2898.
- [8] D. M. McCluskey, T. N. Smith, P. K. Madasu, C. E. Coumbe, M. A. Mackey, P. A. Fulmer, J. H. Wynne, S. Stevenson, J. P. Phillips, *ACS Appl. Mater. Interfaces* **2009**, *1*, 882–887.
- [9] J. D. Wilson, W. C. Broaddus, H. C. Dorn, P. P. Fatouros, C. E. Chalfant, M. D. Shultz, *Bioconjug. Chem.* **2012**, *23*, 1873–1880.
- [10] Y. Yasutake, Z. Shi, T. Okazaki, H. Shinohara, Y. Majima, *Nano Lett.* **2005**, *5*, 1057–1060.
- [11] J. R. Pinzón, D. C. Gasca, S. G. Sankaranarayanan, G. Bottari, T. Torres, D. M. Guldi, L. Echegoyen, *J. Am. Chem. Soc.* **2009**, *131*, 7727–7734.
- [12] Y. Chai, T. Guo, C. Jin, R. E. Haufler, L. P. F. Chibante, J. Fure, L. Wang, J. M. Alford, R. E. Smalley, *J. Phys. Chem.* **1991**, *95*, 7564–7568.
- [13] X. Lu, K. Nakajima, Y. Iiduka, H. Nikawa, N. Mizorogi, Z. Slanina, T. Tsuchiya, S. Nagase, T. Akasaka, *J. Am. Chem. Soc.* **2011**, *133*, 19553–19558.
- [14] D. E. Manolopoulos, P. W. Fowler, *An Atlas of Fullerenes*, Clarendon: Oxford, United Kingdom, **1995**.
- [15] H. W. Kroto, *Nature* **1987**, *329*, 529–531.
- [16] T. Akasaka, T. Wakahara, S. Nagase, K. Kobayashi, M. Waelchli, K. Yamamoto, M. Kondo, S. Shirakura, Y. Maeda, T. Kato, Y. Nakadaira, X. Gao, E. v. Caemelbecke, K. M. Kadish, *J. Phys. Chem. B* **2001**, *105*, 2971–2974.
- [17] K. Muthukumar, J. A. Larsson, *J. Phys. Chem. A* **2008**, *112*, 1071–1075.
- [18] M. Garcia-Borràs, J. M. Luis, M. Swart, M. Solà, *Chem. Eur. J.* **2013**, *19*, 4468–4479.
- [19] M. Garcia-Borràs, S. Osuna, J. M. Luis, M. Swart, M. Solà, *Chem. Soc. Rev.* **2014**, *43*, 5089–5105.
- [20] L. Feng, T. Nakhodo, T. Wakahara, T. Tsuchiya, Y. Maeda, T. Akasaka, T. Kato, E. Horn, K. Yoza, N. Mizorogi, S. Nagase, *J. Am. Chem. Soc.* **2005**, *127*, 17136–17137.

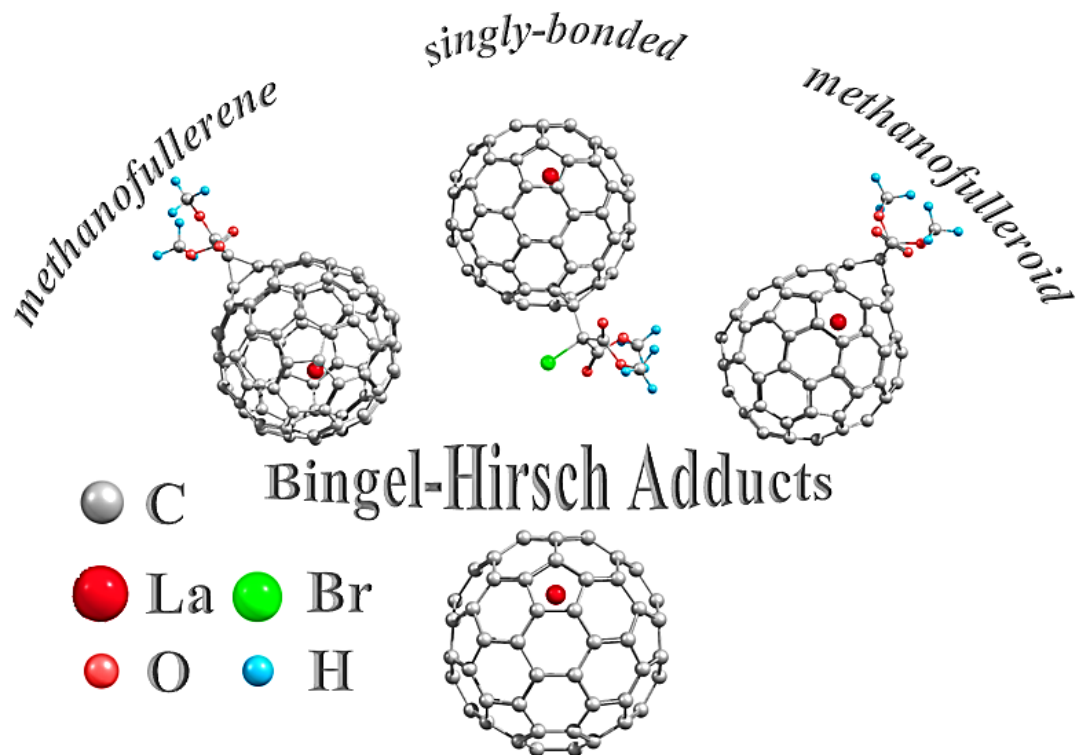
- [21] T. Akasaka, S. Nagase, K. Kobayashi, T. Suzuki, T. Kato, K. Yamamoto, H. Funasaka, T. Takahashi, *J. Chem. Soc. Chem. Commun.* **1995**, 1343–1344.
- [22] R. Valencia, A. Rodríguez-Forteza, J. M. Poblet, *J. Phys. Chem. A* **2008**, *112*, 4550–4555.
- [23] S. Nagase, K. Kobayashi, *Chem. Phys. Lett.* **1993**, *214*, 57–63.
- [24] T. Akasaka, T. Kato, K. Kobayashi, S. Nagase, K. Yamamoto, H. Funasaka, T. Takahashi, *Nature* **1995**, *374*, 600–601.
- [25] J. M. Campanera, C. Bo, J. M. Poblet, *Angew. Chem., Int. Ed.* **2005**, *44*, 7230–7233.
- [26] Y. Maeda, J. Miyashita, T. Hasegawa, T. Wakahara, T. Tsuchiya, L. Feng, Y. Lian, T. Akasaka, K. Kobayashi, S. Nagase, M. Kako, K. Yamamoto, K. M. Kadish, *J. Am. Chem. Soc.* **2005**, *127*, 2143–2146.
- [27] T. Akasaka, T. Wakahara, S. Nagase, K. Kobayashi, M. Waelchli, K. Yamamoto, M. Kondo, S. Shirakura, S. Okubo, Y. Maeda, T. Kato, M. Kako, Y. Nakadaira, R. Nagahata, X. Gao, E. v. Caemelbecke, K. M. Kadish, *J. Am. Chem. Soc.* **2000**, *122*, 9316–9317.
- [28] E. Nishibori, M. Takata, M. Sakata, H. Tanaka, M. Hasegawa, H. Shinohara, *Chem. Phys. Lett.* **2000**, *330*, 497–502.
- [29] Y. Maeda, J. Miyashita, T. Hasegawa, T. Wakahara, T. Tsuchiya, T. Nakahodo, T. Akasaka, N. Mizorogi, K. Kobayashi, S. Nagase, T. Kato, N. Ban, H. Nakajima, Y. Watanabe, *J. Am. Chem. Soc.* **2005**, *127*, 12190–12191.
- [30] C. M. Cardona, A. Kitaygorodskiy, A. Ortiz, M. A. Herranz, L. Echegoyen, *J. Org. Chem.* **2005**, *70*, 5092–5097.
- [31] C. Bingel, *Chem. Ber.* **1993**, *126*, 1957–1959.
- [32] A. Hirsch, I. Lamparth, T. Groesser, H. R. Karfunkel, *J. Am. Chem. Soc.* **1994**, *116*, 9385–9386.
- [33] D. M. Rivera-Nazario, J. R. Pinzón, S. Stevenson, L. A. Echegoyen, *J. Phys. Org. Chem.* **2013**, *26*, 194–205.
- [34] A. F. Kiely, R. C. Haddon, M. S. Meier, J. P. Selegue, C. P. Brock, B. O. Patrick, G.-W. Wang, Y. Chen, *J. Am. Chem. Soc.* **1999**, *121*, 7971–7972.
- [35] R. D. Bolskar, A. F. Benedetto, L. O. Husebo, R. E. Price, E. F. Jackson, S. Wallace, L. J.

- Wilson, J. M. Alford, *J. Am. Chem. Soc.* **2003**, *125*, 5471–5478.
- [36] M. D. Diener, J. M. Alford, S. J. Kennel, S. Mirzadeh, *J. Am. Chem. Soc.* **2007**, *129*, 5131–5138.
- [37] C. M. Cardona, A. Kitaygorodskiy, L. Echegoyen, *J. Am. Chem. Soc.* **2005**, *127*, 10448–10453.
- [38] T. Cai, C. Slebodnick, L. Xu, K. Harich, T. E. Glass, C. Chancellor, J. C. Fettinger, M. M. Olmstead, A. L. Balch, H. W. Gibson, H. C. Dorn, *J. Am. Chem. Soc.* **2006**, *128*, 6486–6492.
- [39] O. Lukoyanova, C. M. Cardona, J. Rivera, L. Z. Lugo-Morales, C. J. Chancellor, M. M. Olmstead, A. Rodríguez-Forteza, J. M. Poblet, A. L. Balch, L. Echegoyen, *J. Am. Chem. Soc.* **2007**, *129*, 10423–10430.
- [40] J. R. Pinzón, T. Zuo, L. Echegoyen, *Chem. Eur. J.* **2010**, *16*, 4864–4869.
- [41] S. Yang, C. Chen, X. Li, T. Wei, F. Liu, S. Wang, *Chem. Commun.* **2013**, *49*, 10844–10846.
- [42] M. N. Chaur, F. Melin, A. J. Athans, B. Elliott, K. Walker, B. C. Holloway, L. Echegoyen, *Chem. Commun.* **2008**, 2665–2667.
- [43] T. Cai, L. Xu, C. Shu, J. E. Reid, H. W. Gibson, H. C. Dorn, *J. Phys. Chem. C* **2008**, *112*, 19203–19208.
- [44] N. Alegret, M. N. Chaur, E. Santos, A. Rodríguez-Forteza, L. Echegoyen, J. M. Poblet, *J. Org. Chem.* **2010**, *75*, 8299–8302.
- [45] N. Alegret, A. Rodríguez-Forteza, J. M. Poblet, *Chem. Eur. J.* **2013**, *19*, 5061–5069.
- [46] M. Garcia-Borràs, S. Osuna, M. Swart, J. M. Luis, L. Echegoyen, M. Solà, *Chem. Commun.* **2013**, *49*, 8767–8769.
- [47] N. Alegret, P. Salvadó, A. Rodríguez-Forteza, J. M. Poblet, *J. Org. Chem.* **2013**, *78*, 9986–9990.
- [48] M. Garcia-Borràs, M. R. Cerón, S. Osuna, M. Izquierdo, J. M. Luis, L. Echegoyen, M. Solà, *Angew. Chem. Int. Ed.* **2016**, *55*, 2374–2377.
- [49] L. Feng, T. Wakahara, T. Nakahodo, T. Tsuchiya, Q. Piao, Y. Maeda, Y. Lian, T.

- Akasaka, E. Horn, K. Yoza, T. Kato, N. Mizorogi, S. Nagase, *Chem. Eur. J.* **2006**, *12*, 5578–5586.
- [50] L. Feng, T. Tsuchiya, T. Wakahara, T. Nakahodo, Q. Piao, Y. Maeda, T. Akasaka, T. Kato, K. Yoza, E. Horn, N. Mizorogi, S. Nagase, *J. Am. Chem. Soc.* **2006**, *128*, 5990–5991.
- [51] Y. Maeda, S. Sato, K. Inada, H. Nikawa, M. Yamada, N. Mizorogi, T. Hasegawa, T. Tsuchiya, T. Akasaka, T. Kato, Z. Slanina, S. Nagase, *Chem. Eur. J.* **2010**, *16*, 2193–2197.
- [52] G. te Velde, F. M. Bickelhaupt, E. J. Baerends, C. Fonseca Guerra, S. J. A. van Gisbergen, J. G. Snijders, T. Ziegler, *J. Comput. Chem.* **2001**, *22*, 931–967.
- [53] M. Swart, J. G. Snijders, *Theor. Chem. Acc.* **2004**, *111*, 56–56.
- [54] J. G. Snijders, M. Swart, *Theor. Chem. Acc.* **2003**, *110*, 34–41.
- [55] E. van Lenthe, E. J. Baerends, J. G. Snijders, *J. Chem. Phys.* **1993**, *99*, 4597–4610.
- [56] A. D. Becke, *Phys. Rev. A* **1988**, *38*, 3098–3100.
- [57] J. Perdew, *Phys. Rev. B* **1986**, *33*, 8822–8824.
- [58] M. Swart, M. Solà, F. M. Bickelhaupt, *J. Comput. Chem.* **2007**, *28*, 1551–1560.
- [59] S. Grimme, J. Antony, S. Ehrlich, H. Krieg, *J. Chem. Phys.* **2010**, *132*, 154104.
- [60] S. Grimme, S. Ehrlich, L. Goerigk, *J. Comput. Chem.* **2011**, *32*, 1456–1465.
- [61] S. Osuna, M. Swart, M. Solà, *J. Phys. Chem. A* **2011**, *115*, 3491–3496.
- [62] A. Klamt, *J. Phys. Chem.* **1995**, *99*, 2224–2235.
- [63] M. Swart, F. M. Bickelhaupt, *J. Comput. Chem.* **2008**, *29*, 724–734.
- [64] M. Swart, F. M. Bickelhaupt, *Int. J. Quantum Chem.* **2006**, *106*, 2536–2544.
- [65] C. P. Kelly, C. J. Cramer, D. G. Truhlar, *J. Chem. Theory Comput.* **2005**, *1*, 1133–1152.
- [66] C. P. Kelly, C. J. Cramer, D. G. Truhlar, *J. Phys. Chem. B* **2006**, *110*, 16066–16081.

- [67] V. S. Bryantsev, M. S. Diallo, W. A. Goddard, *J. Phys. Chem. B* **2008**, *112*, 9709–9719.
- [68] Q.-Z. Li, J.-J. Zheng, X. Zhao, *J. Phys. Chem. C* **2015**, *119*, 26196–26201.
- [69] L. P. Wolters, F. M. Bickelhaupt, *WIREs Comput. Mol. Sci.* **2015**, *5*, 324–343.
- [70] F. M. Bickelhaupt, *J. Comput. Chem.* **1999**, *20*, 114–128.
- [71] I. Fernández, F. M. Bickelhaupt, *Chem. Soc. Rev.* **2014**, *43*, 4953–4967.
- [72] K. N. Houk, R. W. Gandour, R. W. Strozier, N. G. Rondan, L. A. Paquette, *J. Am. Chem. Soc.* **1979**, *101*, 6797–6802.
- [73] D. H. Ess, K. N. Houk, *J. Am. Chem. Soc.* **2007**, *129*, 10646–10647.
- [74] Y. Cao, Y. Liang, L. Zhang, S. Osuna, A.-L. M. Hoyt, A. L. Briseno, K. N. Houk, *J. Am. Chem. Soc.* **2014**, *136*, 10743–10751.
- [75] M. Cases, M. Duran, J. Mestres, N. Martín, M. Solà, *Fullerenes for the New Millennium*, P. V. Kamat, K. M. Kadish, D. M. Guldi, Eds., The Electrochemical Society Inc., Pennington, **2011**, *11*, 244–269.
- [76] C. Shu, T. Cai, L. Xu, T. Zuo, J. Reid, K. Harich, H. C. Dorn, H. W. Gibson, *J. Am. Chem. Soc.* **2007**, *129*, 15710–15717.
- [77] C. Fonseca Guerra, J.-W. Handgraaf, E. J. Baerends, F. M. Bickelhaupt, *J. Comput. Chem.* **2004**, *25*, 189–210.

Table of contents



Keywords: Bingel-Hirsch reaction, endohedral metallofullerenes, regioselectivity, reaction mechanism, La@C_{2v}-C₈₂, density functional theory